J Eng Math (2009) 65:221–228
DOI 10.1007/s10665-009-9306-y

Free-surface stability of a damped thin-film flow

D. Molenaar

Received: 11 May 2007 / Accepted: 15 June 2009 / Published online: 2 July 2009

Abstract An idealized model is presented, describing the flow of a thin film through a dilute porous layer of immobile obstacles. Damping due to the obstacles extends the linear stability of the flow, where the depth-integrated flowrates retrieved at each order of the film expansion are expressed in terms of hyperbolic functions. Three-dimensional numerical simulations reveal a transition from steepening waves to stationary travelling waves for increasing values of the damping parameter.

Keywords Linear stability · Lubrication · Porous media · Thin-film flows

1 Introduction

Thin-film flows over rough substrates or through porous layers, in which the motion of the fluid is partially impeded by the presence of solid obstacles, occur in many settings. Examples include the manufacturing of magnetic storage devices [1,2], the extraction of a porous layer from a fluid bath [3], lubrication of journal bearings [4], flows over rough soil surfaces [5,6], flows through polymer brushes [7] and absorption processes in heat exchangers [8,9]. As opposed to flows past a limited number of obstacles [10–12], where a computation of instantaneous velocities may be feasible, porous layers contain a large number of obstacles and the fluid velocity must be averaged over a small control volume or over many possible configurations of the obstacles contained within the porous layer.

The present study is concerned with the free-surface stability of a gravity-driven thin film flowing through a dilute porous layer. The porous layer, with a thickness that is of the same order as the film thickness, is attached to an impermeable substrate and the film is bound in the thin direction by the substrate and by a free liquid–air interface. Obstacles contained in the porous layer are assumed to be neutrally wetting and consequently no meniscii develop around individual obstacles piercing the free surface. Dissipation due to moving liquid–solid contact lines can thus be ignored. Taking both inertial and surface-tension effects into account, our main interest is in the stability and evolution of the free film surface as a function of the strength of damping of the flow due to the presence of the porous layer.

An example of a dilute porous medium is a fibrous filter or polymer brush [7]. Fibrous porous media are characterized by low solid-mass fractions, $0.0001 < \phi < 0.1$ [13,14]. The solid-mass fraction in fibrous layers is

D. Molenaar (✉)
Physics of Geological Processes, University of Oslo, P. O. Box 1048, 0316 Blindern, Oslo, Norway
e-mail: davidmolenaar@gmail.com

proportional to the averaged fiber properties, $\phi \propto a^2/L_{\text{fiber}}^2$, with average separation length L_{fiber} and fiber radius a, and in a dilute layer, fiber radii are much smaller than the average fiber separation length, $a \ll L_{\text{fiber}}$.

Due to the dilute nature of the porous layer, viscous and inertial effects are assumed to be non-negligible [8,9], in contrast to the usual situation in dense porous media. The drag of the obstacles upon the flow is coarse-grained in the form of a linear Darcy damping term in the equations of motion, which take the form of the nonlinear Brinkman equations. Originally posed for a dilute porous medium of spherical grains, Brinkmans' linear model [15] was later extended to incorporate inertial effects to describe, for instance, flow problems on porous-fluid interfaces [16], Berman channel flow [17] and thermal convection in a fluid layer overlying a porous medium [18].

Here, the nonlinear Brinkman equations form the starting point for a thin-film approximation, in which the liquid pressure and velocity are expanded in terms of a small parameter. These fields are then enslaved to the film thickness, which becomes the effective degree of freedom of the model. At each order of the thin-film expansion the depth-integrated flowrate can be expressed in terms of hyperbolic functions of the film thickness. The resulting damped thin-film model, Eq. 14 in Sect. 2, is a strongly nonlinear Benney-type equation describing the evolution of the free surface of the film.

Although the first step of the expansion leading to our model overlaps with the quasilinear film model presented in [5,6], the emphasis in the present work is on the free-surface stability of the film, where the contribution of inertial terms and the effect of surface tension at the liquid–air interface play an important role. The non-dimensional parameter which guides the strength of inertial effects is the effective Reynolds number, Re, and the validity criterium for the film expansion demands that Re is of order unity. The effect of surface tension at the liquid–air interface is measured by the effective inverse capillary number, Ca. However, the focus here is on the inverse Darcy number, λ, which controls the strength of damping of the flow and scales with the (inverse) permeability of the porous layer. The range of linear stability of the flow increases as a function of the inverse Darcy number, as discussed in Sect. 3.1, below. Beyond the linear regime, three-dimensional numerical results for the strongly nonlinear model are presented in Sect. 3.2, where the evolution of the film thickness over time, starting from an initial long-wave perturbation of finite amplitude, is monitored. Finally, Sect. 4 contains the conclusions.

2 Model equation

Suppose a thin fluid film flows through a dilute layer of immobile obstacles placed on a rigid surface. The substrate is inclined at an angle θ with respect to the horizontal, sustaining a gravity-driven flow. Obstacles are assumed to be neutrally wetting, such that no meniscus develops at the solid-fluid boundary on individual obstacles. Coordinate x denotes the streamwise (downslope) direction along the substrate, y denotes the spanwise direction and z denotes the thin (surface normal) direction. The fluid is incompressible,

$$\nabla \cdot \mathbf{u} = 0, \tag{1}$$

where the velocity $\mathbf{u} = (u, v, w)$ is an ensemble averaged velocity, averaged over all possible configurations of the obstacles. The momentum balance then takes the form of the Navier–Stokes equations of Brinkman type [15,19],

$$\mu \Delta \mathbf{u} - \frac{\mu}{K}\mathbf{u} = \nabla p - \rho \hat{\mathbf{g}} + \rho(\mathbf{u} \cdot \nabla \mathbf{u} + \partial_t \mathbf{u}), \tag{2}$$

with gravity vector $\hat{\mathbf{g}} = g(\sin\theta, 0, \cos\theta)$, fluid density ρ and permeability coefficient K. At the free surface of the film, $z = h(t, x, y)$, there is a balance of stresses in the normal direction, $\mathbf{n} \cdot \Pi \cdot \mathbf{n} = \sigma\kappa$, and in the tangential direction, $\mathbf{t} \cdot \Pi \cdot \mathbf{n} = 0$. Here, σ is the surface-tension coefficient, κ is the local curvature of the free film surface, and the unit normal and tangent vectors at the free surface are $\mathbf{n}$ and $\mathbf{t}$, respectively. The stress tensor reads as $\Pi = \mu[\nabla\mathbf{u} + (\nabla\mathbf{u})^T] - p\mathbf{I}$, with unit tensor $\mathbf{I}$. As the obstacles are neutrally wetting, effects of moving contact lines at obstacles piercing the free surface can be ignored. Further study is required to extend the free-surface boundary conditions above to include such effects.

The evolution of the film surface follows from the kinematic condition,

$$\partial_t h + \nabla \cdot \int_0^h \mathbf{u} \mathrm{d}z = 0, \tag{3}$$

which forms the basis for the thin-film equation. Referring to the special geometry of the film, the characteristic scale in the thin direction, H, is an order of magnitude smaller than the characteristic scale in the planar directions, L, such that the ratio of these scales defines a small parameter, $\epsilon = H/L \ll 1$, also referred to as the longwave assumption [20]. Hence, coordinates x and y are scaled with L, while z and h are scaled with the characteristic thickness H. In gravity-driven systems a natural choice for the characteristic planar velocity scale follows from the lowest-order (Nusselt) solution, $U = \rho g H^2/\mu$ [20]. Assuming that the terms $\partial_x u$, $\partial_y v$ and $\partial_z w$ in the mass balance (1) are all of equal magnitude, it follows that the characteristic velocity scale in the thin direction of the film is an order of magnitude smaller than the planar velocity scale, $W = \epsilon U$. The pressure scale is $P = \mu U L/H^2$, which, with the planar velocity scale, equals $P = \rho g L$. Dividing Eq. 2 by ρg, it is seen that the inertial terms are scaled by ϵRe, where the effective Reynolds number $\mathrm{Re} = \epsilon \rho U L/\mu$, is of order unity, $\mathrm{Re} = \mathcal{O}(1)$. Damping terms scale with the inverse Darcy number, $\lambda = \mu U/\rho g K$. With the expression for the planar velocity scale U, the damping parameter becomes

$$\lambda = H^2/K. \tag{4}$$

Given that H and ϵ remain small enough to be in the thin-film regime, the limit of diverging permeability, or $\lambda \to 0$, corresponds to an unimpeded flow. For a dense porous layer the permeability vanishes, with $\lambda \to \infty$, and inertial effects become negligible. In [21] it was argued that in the latter limit the time-dependent and viscous terms should be modified, whereas the inertial terms should be replaced by a quadratic, Forchheimer drag. Consequently, the present study is limited to the case of a dilute porous layer. In fibrous layers the permeability is proportional to the average fiber spacing $K^{1/2} \propto L_{\mathrm{fiber}}$ such that the inverse Darcy number scales as $\lambda \propto H^2/L^2_{\mathrm{fiber}}$. For instance, in an ordered square array of cylindrical fibers the permeability roughly equals $K \simeq L^2_{\mathrm{fiber}}/25$ [14] and the inverse Darcy number in such an array becomes $\lambda \simeq 25 H^2/L^2_{\mathrm{fiber}}$. Because the flows considered here are in the thin-film regime, the value of parameter λ may well be smaller than unity. For instance, using water as a working fluid and an effective Reynolds number Re = 1, with $\epsilon = 0.1$, the characteristic film thickness scale equals $H = 10^{-13/3}$. With the latter estimate, the values of the damping parameter for the porous layer heat exchangers considered in [8,9], are within the range $0.44 \leq \lambda \leq 300.0$. In [6] the values of the damping parameter used for comparison with experimental results range from $\lambda = 1.0 \times 10^{-4}$ to $\lambda = 49.0$.

In the thin-film approximation the velocity components and pressure are expanded in the film parameter, e.g., $u = u^{(0)} + \epsilon u^{(1)} + \epsilon^2 u^{(2)} + \cdots$. As $W \ll U$ the lowest-order contribution in the thin direction vanishes, $w^{(0)} = 0$. Substituting the expansions in the non-dimensional mass and momentum balances, one obtains systems of ODEs in z at each order of ϵ. These systems are directly integrable, yielding expressions for the velocity components at each order, although the number of terms which is retrieved at one order and has to be plugged into the ODEs at the next order rapidly becomes unmanageable for higher orders of the expansion. Adding higher orders to the expansion increases the accuracy of the solution, however, at the cost of a reduced radius of convergence, where the radius of convergence is related to the Reynolds number of the flow [22,23]. No-slip boundary conditions apply at the substrate, whereas the balance of stresses at the free surface yields a stress-free condition, at orders $i = 0, 1$,

$$\mathbf{u}^{(i)}|_{z=0} = 0 \quad \text{and} \quad \partial_z \mathbf{u}^{(i)}|_{z=h} = 0. \tag{5}$$

Collecting terms at order zero, one may reduce the momentum balances in the thin and spanwise directions to

$$\partial_z p^{(0)} = 0 \quad \text{and} \quad \{\partial_{zz} - \lambda\} v^{(0)} = \partial_y p^{(0)}. \tag{6}$$

When the atmospheric pressure at the free surface is set to zero, integration yields $p^{(0)} = 0$, and, with the boundary conditions (5), $v^{(0)} = 0$. In the downslope direction one retrieves an inhomogeneous Sturm–Liouville problem

$$\{\partial_{zz} - \lambda\} u^{(0)} = \partial_x p^{(0)} - \sin\theta. \tag{7}$$

Integrating the solution of (7) over the film thickness and applying boundary conditions, shows that the flowrate at lowest order $B_\lambda(h) = \int_0^h u^{(0)} \mathrm{d}z$, equals

$$B_\lambda(h) = (\lambda^{-1} h - \lambda^{-3/2} \tanh \lambda^{1/2} h) \sin\theta. \tag{8}$$

The expression for the lowest-order flowrate (8) was derived in [6] for a split-layer flow over a rough surface, where (8) follows from [6, Eq. 7], by setting the roughness height k equal to the film thickness h. In the limit of an unimpeded flow with zero damping, $\lambda = 0$, the flowrate equals $\frac{1}{3}h^3$ [24], which can easily be observed from a Taylor expansion of (8), $B_\lambda(h) = \frac{1}{3}h^3 - \frac{2}{15}\lambda h^5 + \mathcal{O}(\lambda^2 h^7)$. Without damping terms, Eq. 3 reduces to a version of the Burgers equation, describing wave-steepening and gradient amplification. Damping counteracts the gradient amplification, leading to higher-order corrections to the cubic flowrate of a non-damped flow, where the leading damping-related term is quintic in h.

Gradient-limiting surface-tension terms are assumed to enter the thin-film approximation below their formal (third) order [20,24], preventing wave-steepening and shocks, which would be incompatible with the longwave expansion. The surface-tension terms enter through the linearized boundary conditions on the pressure at the free-film surface, for which one assumes that the planar gradient of h satisfies $|\nabla_p h|^2 \ll 1$.

The first-order pressure contribution then follows from an integration of the momentum balance in the thin direction,

$$\partial_z p^{(1)} = \cos\theta, \tag{9}$$

obtaining

$$p^{(1)}(t, \mathbf{x}) = (h - z)\cos\theta - (\epsilon \mathrm{Ca})\Delta h. \tag{10}$$

Here, the surface-tension term scales with the effective inverse capillary number, $\mathrm{Ca} = \epsilon^2\sigma/\mu U$. If one takes the planar length scale equal to the capillary length $L = (\sigma/\rho g)^{1/2}$, one sees, with the definitions for U and ϵ, that the effective inverse capillary number equals unity and the surface-tension term is of first order in ϵ. Plugging the components $u^{(0)}$, $v^{(0)}$ and $w^{(1)}$ into the continuity balance (1) and multiplying by H, one finds that the remaining non-zero terms are of equal (first) order in ϵ. Velocity component $w^{(1)}$ then follows from integrating, $w^{(1)} = -\int_z \partial_x u^{(0)} \mathrm{d}z$. Next, the Sturm–Liouville problems for the planar velocity components at first order become

$$\{\partial_{zz} - \lambda\}u^{(1)} = \partial_x p^{(1)} + \mathrm{Re}\{u^{(0)}\partial_x + w^{(1)}\partial_z + \partial_t\}u^{(0)} \text{ and } \{\partial_{zz} - \lambda\}v^{(1)} = \partial_y p^{(1)}, \tag{11, 12}$$

complemented with boundary conditions (5), where the non-zero first-order pressure contribution sustains a non-vanishing velocity component in the lateral direction. Note that the time derivative of $u^{(0)}$ in the right-hand side of (11) leads to the appearance of the time derivative of h in the problem, for which the lowest-order estimate, $\partial_t h = -\partial_x \int_0^h u^{(0)} \mathrm{d}z$, can be substituted. Integration of (11) and (12), leads to the flowrate

$$\int_0^h (u^{(1)}, v^{(1)})\mathrm{d}z = \mathrm{Re}A_\lambda(h)\partial_x h\hat{\mathbf{e}}_x - B_\lambda(h)\nabla(h\cot\theta - \mathrm{Ca}\Delta h) \tag{13}$$

for unit vector $\hat{\mathbf{e}}_x = (1, 0)$. The flowrate contains a pressure contribution, with amplitude $B_\lambda(h)$, and an inertial contribution in the x-direction, with amplitude

$$A_\lambda(h) = \lambda^{-3}\mathrm{Re}\left\{\frac{\sinh\xi}{\cosh^3\xi}\left[\xi - \tanh\xi - \sinh\xi + \tfrac{1}{4}\sinh 2\xi + \tfrac{1}{2}\xi\,\mathrm{sech}^2\xi\right] + \tfrac{1}{2}\mathrm{sech}^4\xi - \mathrm{sech}^3\xi + \mathrm{sech}\xi - \tfrac{1}{2}\right\},$$

where $\xi = \lambda^{1/2}h$, for brievety of notation. For unimpeded flows the leading term due to inertial effects has an amplitude equal to $\frac{2}{15}h^6$ (see [20,24]) which can also be observed from an expansion of the amplitude of the inertial contribution, $A_\lambda(h) = \frac{2}{15}h^6 - \frac{2187}{5040}\lambda h^8 + \mathcal{O}(\lambda^2 h^{10})$. The leading correction due to damping is an octic term in the film thickness. A combination of flowrates (8) and (13) gives the evolution equation for the film surface

$$\partial_t h + \nabla\cdot[B_\lambda(h)\hat{\mathbf{e}}_x + \epsilon\mathrm{Re}A_\lambda(h)\partial_x h\hat{\mathbf{e}}_x + \epsilon B_\lambda(h)\nabla(\mathrm{Ca}\Delta h - h\cot\theta)] = 0; \tag{14}$$

this is a fourth-order nonlinear equation that reduces to the Benney equation for zero damping, $\lambda = 0$. For large values of the inverse Dacy number, corresponding to dense porous layers, the thin-film model (14) eventually breaks down. In the latter case the length scale associated with the porous obstacles becomes dominant over the characteristic film length L and one can no longer guarantee that velocity components in the stream- and spanwise directions are an order of magnitude larger than the velocity component in the thin direction. In addition, for a dense

porous layer the nonlinear Brinkman model loses validity and should be replaced by a model without inertial terms and with an additional quadratic drag term [21]. To meet these validity criteria, the values of λ considered below correspond to a dilute porous medium, $\lambda \leq 10$. Finally, the validity of the thin-film expansion is limited to small inertial effects, for which $\epsilon \mathrm{Re} \ll 1$ (see [23]); this point is further discussed in Sect. 3.2.

3 Stability

3.1 Linear analysis

Consider the linear stability of the damped thin-film model, splitting the non-dimensional film thickness into a constant base value, H_0, and a small perturbation, $h' \ll H_0$, and substituting this decomposition in (14). For wavenumber vector (α, β) and temporal growthrate Ψ, the decomposition reads as $h(t, x, y) = H_0 + h' \exp(\mathrm{i}(\alpha x + \beta y) + \Psi t)$. Linearizing in h' and keeping only the real part of the growth rate yields

$$\Psi = \epsilon \mathrm{Re} A_\lambda(H_0)\alpha^2 - \epsilon B_\lambda(H_0)(\alpha^2 + \beta^2)[\cot\theta + \mathrm{Ca}(\alpha^2 + \beta^2)]. \tag{15}$$

In unimpeded film flows, instabilities can only occur if the film thickness exceeds the critical value $\frac{2}{5}H_c^3 = \cot\theta$, where the cubic term H_c^3 is related to the effective Reynolds number [20]. Hence, falling films on vertical substrates, $\theta = \pi/2$, are always unstable. In contrast, damped flows may be linearly stable even on a vertical substrate.

Growth rates for a two-dimensional flow ($\beta = 0$) on a vertical substrate are shown in Fig. 1a, for several values of the inverse Darcy number and for Ca = 1.0 and Re = 1.0. Instability and growth of small perturbations occur in the area enclosed by each curve and the ($\Psi = 0$)-axis, where instability follows from a competition between the fourth-order (damping) surface-tension terms and the second-order (amplifying) inertial terms. Increasing the strength of damping due to the porous layer results in a flattening of the instability region, where the critical wavenumber, α_c, at which zero growth occurs, decays rapidly as a function of the inverse Darcy number. The critical wavenumber obeys the relation

$$\alpha_c = \mathrm{Ca}^{-1/2}(\mathrm{Re}\delta_\lambda(H_0) - \cot\theta)^{1/2} \tag{16}$$

for ratio $\delta_\lambda(H_0) = A_\lambda(H_0)/B_\lambda(H_0)$ and the corresponding decay of α_c as a function of the inverse Darcy number is shown in Fig. 1b. The stability condition for the damped case follows from (16), for critical base thickness H_c,

$$\mathrm{Re}\delta_\lambda(H_c) = \cot\theta. \tag{17}$$

In the limit $\lambda \to 0$ one retrieves $\delta_\lambda(H_c) \to \frac{2}{5}H_c^3$, which is evident from the Taylor expansions for $A_\lambda(h)$ and $B_\lambda(h)$, discussed in the previous section.

3.2 Numerical results

The nonlinear regime of the damped-film model is explored by means of three-dimensional numerical simulations, computing the evolution of the film surface on a vertical substrate and starting with an initial finite-amplitude perturbation. Using a finite-difference scheme and applying spatial-direction splitting, known as the alternate-direction implicit (ADI) technique, as described in [25], the fourth-order problem (14) is solved on a square domain. ADI techniques allow for relatively large time steps without causing numerical stability problems, here using $\delta t = 2 \times (\delta x)^3$, for spatial discretization step δx. Periodic boundary conditions are applied in the downslope and lateral directions, mimicking a flow with a constant base thickness.

The initial field comprises a single longwave perturbation of small amplitude, imposed upon a constant base thickness,

$$h(0, x, y) = H_0 + 0.01 \sin(2\pi x/D) \sin(2\pi y/D) \tag{18}$$

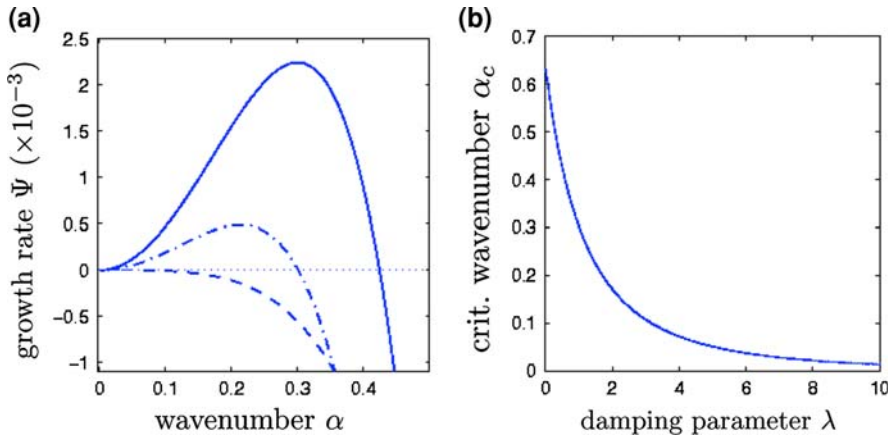

Fig. 1 Neutral two-dimensional stability curves (**a**) on a vertical substrate, as a function of wavenumber α. Positive growth rates Ψ of small perturbations are enclosed between the curves and the ($\Psi = 0$)-axis. Three curves are shown for inverse Darcy numbers $\lambda = 0.5$ (*solid line*), $\lambda = 1.0$ (*dash–dotted line*) and $\lambda = 10.0$ (*dashed line*). The critical wavenumber occurs at the intersection of each curve with the ($\Psi = 0$)-axis. Decay of the critical wavenumber α_c, as a function of the damping parameter λ (**b**). In both figures Ca = 1.0 and Re = 1.0

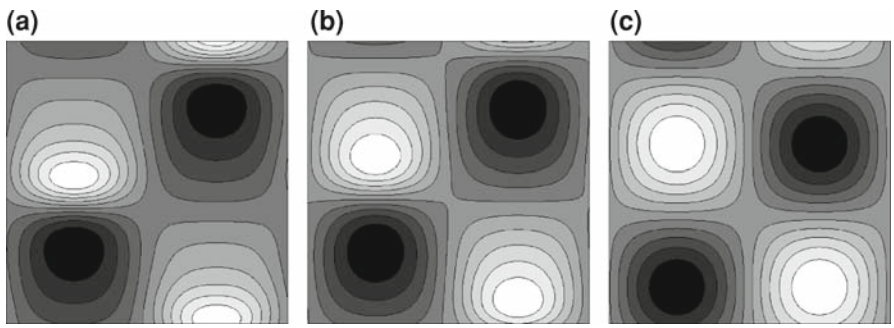

Fig. 2 Contour plots of the free surface at $t = 61.0$, for three values of the inverse Darcy number; $\lambda = 0.01$ (**a**), $\lambda = 1.0$ (**b**) and $\lambda = 10.0$ (**c**). Shown are ten equidistant contour levels, ranging from $h = 0.99$ (*black*) to $h = 1.01$ (*white*). The downslope direction is from top to bottom in the figures, where the domain length equals $D = 5L$ in both directions

for domain length $D = 5L$ and base thickness $H_0 = 1$. Using water as the working fluid, other parameter values are chosen as follows $\epsilon \mathrm{Re} = 0.1$ with $\epsilon = 1.87 \times 10^{-2}$ and $\epsilon \mathrm{Ca} = 3.0 \times 10^{-4}$. The number of grid points equals $N = 80$ in both directions and the time step is $\delta t = 5.0 \times 10^{-4}$.

Snapshots of the film surface at $t = 61.0$, corresponding to 1.25×10^5 time steps, are shown in Fig. 2 for several values of the damping parameter λ. When the values of the effective capillary and Reynolds numbers are fixed, the numerical results reveal the presence of two regimes. In the weakly damped regime, for low values of the damping parameter, $\lambda \leq 1$, the initial long-wavelength perturbation develops into a pattern of steepening waves, as shown in Fig. 2a, b. Initial wave tops develop into steep bulges, initial wave throughs flatten out. A downslope cross-section of the film thickness at several times shows the steepening process in Fig. 3, where the cross-section at $t = 61.0$ is taken from Fig. 2c.

For progressively larger values of the inverse Darcy number, the wave steepening process becomes progressively weaker. When the flow is strongly damped, for instance, at inverse Darcy number $\lambda = 10$, a pattern of travelling waves occurs, where the initial perturbation remains stationary with respect to a moving frame of reference; Fig. 2c. Simulations running over longer times, up to $t = 244.0$, did not reveal late-time wave-steepening in the strongly damped regime.

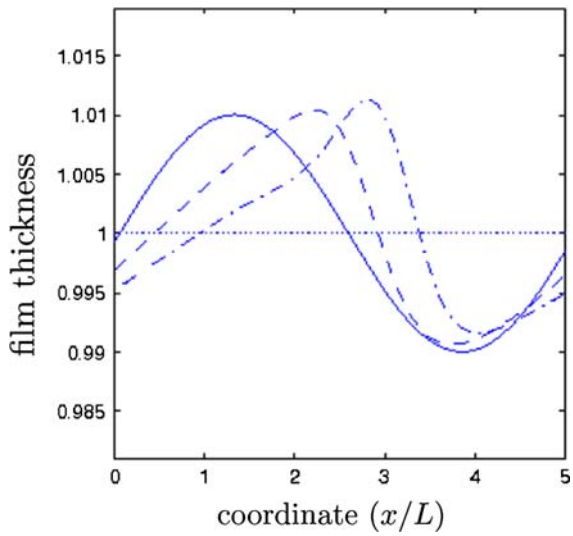

Fig. 3 Evolution of the free surface, shown with consecutive thickness profiles, taken along the line $y = D/4$, along the downslope direction of the domain for $t = 0.0$ (*solid line*), $t = 32.5$ (*dashed line*) and $t = 61.0$ (*dash–dotted line*)

For the undamped ($\lambda = 0$) Benney equation, there exists a critical Reynolds number, above which finite-time blow-up of solutions occurs [22,23]. The unphysical blow-up is a consequence of the strong nonlinearity introduced by the expansion of the inertial terms. The demand on the Reynolds number for the thin-film approximation to be valid is, hence, $\epsilon \mathrm{Re} \ll 1$. Initial simulations with larger Reynolds number ($\epsilon \mathrm{Re} > 1$) for the damped model still show a blow-up. However, the exact stability criterium as a function of the damping parameter remains to be determined. In this respect, interesting results are presented in [6], where a quasilinear version of (14) was used to model flows with Reynolds numbers up to Re = 466.

4 Conclusions

A thin-film model is presented, describing the flow of a thin liquid film through a dilute porous layer and incorporating both nonlinear effects and the effects of surface tension at the free liquid–air interface. At each order of the small-parameter expansion on which the model is based, the flowrate is expressed in terms of hyperbolic functions of the film thickness.

The presence of the dilute porous layer results in an extended linear stability regime of the film, where, as opposed to an unimpeded film flow, a damped flow on a vertical substrate may be linearly stable.

Numerical simulations, starting from a longwave initial perturbation, reveal the presence of two types of solutions. For small values of the inverse Darcy number, corresponding to weak damping, patterns of steepening waves are observed. For larger values of the inverse Darcy number, corresponding to stronger damping, the initial perturbation is preserved and forms a periodic pattern of travelling waves.

Future study may establish for which values of the damping parameter the cross-over from the former to the latter pattern occurs and how the critical value of the Reynolds number, associated to a finite-time blow-up, evolves as a function of the damping parameter.

Acknowledgement The research center PGP is funded by the Norwegian Research Council.

References

1. Li W-L, Wang CC (1999) Derivation of the modified molecular gas lubrication equation—a porous media model. J Phys D Appl Phys 32:1421–1427

2. Lin J-R, Lu R-F, Yang C-B (2001) Derivation of porous squeeze-film Reynolds equations using the Brinkman model and its application. J Phys D Appl Phys 34:3217–3223
3. Devauchelle O, Josserand C, Zaleski S (2007) Forced dewetting on porous media. J Fluid Mech 574:343–364
4. Chen M-D, Chang K-M, Lin J-W, Li W-L (2002) Lubrication of journal bearings—influence of stress jump condition at the porous-media/fluid film interface. Tribol Int 35:287–295
5. Myers T (2002) Modelling laminar sheet flow over rough surfaces. Water Resour Res 38:1230–1242
6. Myers T (2003) Unsteady laminar flow over a rough surface. J Eng Math 46:111–126
7. Anderson JL, McKenzie PF, Webber RM (1991) Model for hydrodynamic thickness of thin polymer layers at solid/liquid interfaces. Langmuir 7:162–166
8. Yang R, Jou D (1995) Heat and mass transfer of absorption process for the falling film flow inside a porous medium. Int J Heat Mass Transf 38:1121–1126
9. Yang R, Jou D (2001) The effect of non-absorbable gas on an absorption process for the falling film flow inside a porous medium. Int J Heat Mass Transf 44:1259–1266
10. Hayes M, O'Brien SGB, Lammers JH (2000) Green's function for steady flow over a small two-dimensional topography. Phys Fluids 12:2845–2858
11. Gaskell PH, Jimack PK, Selleir M, Thompson HM, Wilson MCT (2004) Gravity-driven flow of continuous thin liquid films on non-porous substrates with topography. J Fluid Mech 509:253–280
12. Kondic L, Diez J (2004) Instabilities in the flow of thin films on heterogeneous surfaces. Phys Fluids 16:3341–3360
13. Tachie MF, James DF, Curry IG (2003) Velocity measurements of a shear flow penetrating a porous medium. J Fluid Mech 493:319–343
14. James DF, Davis AMJ (2001) Flow at the interface of a model fibrous medium. J Fluid Mech 426:47–72
15. Brinkman HC (1947) A calculation of the viscous force exerted by a flowing fluid on a dense swarm of particles. Appl Sci Res A 1:27–34
16. Goyeau B, Lhuillier D, Gobin D, Velarde MG (2003) Momentum transport at a fluid-porous interface. Int J Heat Mass Transf 46:4071–4081
17. Deng C, Martinez DM (2005) Linear stability of Berman flow in a channel partially filled with a porous medium. Phys Fluids 17:024102-1–024102-8
18. Desaive Th, Lebon G, Hennenberg M (2001) Coupled capillary and gravity-driven instability in a liquid film overlying a porous layer. Phys Rev E 64:066304-1–066304-8
19. Nield DA, Bejan A (1998) Convection in porous media. Springer, New York
20. Oron A, Davis SH, Bankoff SG (1997) Long-scale evolution of thin liquid films. Rev Mod Phys 69:931–980
21. Nield DA (1991) The limitations of the Brinkman-Forchheimer equation in modeling flow in a saturated porous medium and at an interface. Int J Heat Fluid Flow 12:269–272
22. Scheid B, Ruyer-Quil C, Thiele U, Kabov O, Legros JC, Colinet P (2005) Validity domain of the Benney equation including Marangoni effect for closed and open flows. J Fluid Mech 527:303–335
23. Colinet P, Kaya H, Rossomme S, Scheid B (2007) Some advances in lubrication-type theories. Eur Phys J Spec Top 146:377–389
24. Ruyer-Quil C, Manneville P (1998) Modeling film flows down inclined planes. Eur Phys J B 6:277–292
25. Witelski TP, Bowen M (2003) ADI schemes for higher-order nonlinear diffusion equations. Appl Num Math 45:331–351